A.6 Diffusion & dispersion process

River Flow 2012 – Murillo (Ed.)
© 2012 Taylor & Francis Group, London, ISBN 978-0-415-62129-8

The influence of bed roughness on the dynamics of gravity currents

H.I.S. Nogueira
Department of Civil Engineering & IMAR-CMA, University of Coimbra, Coimbra, Portugal

C. Adduce
Department of Civil Engineering, University of "Roma Tre", Rome, Italy

E. Alves
National Laboratory of Civil Engineering, Lisbon, Portugal

M.J. Franca
Department of Civil Engineering & IMAR-CMA, New University of Lisbon, Caparica, Portugal

ABSTRACT: The present work experimentally investigates the dynamics of unsteady gravity currents over rough beds performed by lock-release of saline water into a fresh water tank. Four experiments were performed by varying roughness throughout the channel bed, maintaining the initial density of the saline water in the lock, the lock length and the water depth. An image analysis technique was applied to visualize and characterize the current allowing thus the understanding of its general dynamics and, more specifically, of the current head dynamics. The convergence of local Froude number obtained at the head suggests that the dynamics, namely entrainment processes, are governed by local variables at the head. The temporal evolution of the head length and mass shows repeated cycles of stretching and breaking, and the average period of the breaking cycles is seen to increase with roughness. The growing rate of the head mass is seen to decrease in time, suggesting that the entrainment at the head is ruled by local buoyancy.

1 INTRODUCTION

Gravity or density currents are flows driven by density differences within a fluid which can be due to temperature differences, dissolved substances or particles in suspension. Releases of pollutant materials into rivers, oil spillage on the sea environment and desalination plant outflows are a few of man-made gravity currents that occur in water masses and frequently cause negative environmental impacts whereas in nature one may observe oceanic fronts, saline plumes, underwater debris flow and turbidity currents. Several examples of gravity currents in the nature can be found comprehensively in Simpson (1997).

The loss of storage in reservoirs, related to the deposition of fine sediments due to turbidity currents, is a subject of great concern to hydraulic engineers and still a topic of research nowadays (Alves et al. 2008, Rossato & Alves 2011); several practical measures have been applied over the years to control sedimentation within reservoirs (Fan & Morris 1992a, b, Kantoush et al. 2010) and innovative solutions are still being investigated (Oehy & Schleiss 2007). Therefore, the understanding of the mechanisms underlying this phenomenon, especially on what concerns mass transfer between the current and ambient fluid, is of extreme importance for the development of prevention measures against its eventual adverse effects.

Density currents have been investigated by both experimental (Rottman & Simpson 1983, Parker et al. 1986, Altinakar 1993, Marino et al. 2005) and numerical modeling (Härtel et al. 2000, Ooi et al. 2007, Paik et al. 2009; Bombardelli et al. 2009).

Several studies have been based on image analysis technique to investigate the dynamics of gravity currents (Shin et al. 2004, Marino et al. 2005, La Rocca et al. 2008, Adduce et al. 2012 in press); the present research, based on experimental work, uses similar techniques (Nogueira et al. 2011). Most of the investigation efforts concern flows developing over smooth beds, though a few investigators have studied the effect of bed roughness on density currents dynamics. Peters & Venart (2000) used Laser-Induced Fluorescence (LIF) to investigate flow dynamics and mixing processes of gravity currents in the head region over rough surfaces. They used regular squared cross-section elements spanning the full channel width with four different side dimensions to produce bed roughness. In general, they observed that roughness decreases the front velocity and induces higher dilution in the head region due to extra entrainment of ambient fluid trapped between roughness

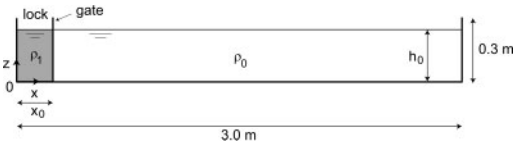

Figure 1. Longitudinal view of the Perspex channel.

elements. Adduce et al. (2009) performed experiments with rough bed using quartz sand and through image analysis technique have also observed that the bed roughness induced a reduction in the front velocity.

The effect of bed roughness in overflows, i.e, dense currents developing downslope in the ocean and important in the ocean circulation system, was numerically investigated by Özgökmen & Fischer (2008). The results of their simulations suggest that roughness enhances drag, with effects on the velocity field, and mixing between the current and ambient fluid, modifying the density distribution within the current.

Despite the previous contributions, the effect of the bed roughness in the dynamics of the head of gravity currents is yet far from being completely explored. Therefore, the present work aims at characterizing the effect of bed roughness on the development of gravity currents, namely in the head region, through lock-exchange experiments.

After this brief introduction, the experimental details are presented in section 2, the main results are summarized in section 3 and, finally, section 4 presents the main conclusions of this work.

2 EXPERIMENTAL DETAILS

The experiments were carried out at the Hydraulics Laboratory of University of Rome, "Roma Tre", in a 3.0 m long transparent Perspex channel with a 0.2 m wide and 0.3 m deep rectangular cross-section with horizontal bed (Fig. 1).

A vertical sliding gate is placed in the channel at a distance $x_0 = 0.15$ m from the left wall to form a lock. The right side of the channel is filled with fresh water with density $\rho_0 = 1000\,\mathrm{kgm^{-3}}$, whereas the lock is filled with saline water with density $\rho_1 = 1030\,\mathrm{kgm^{-3}}$; both sides were filled up at same depth, $h_0 = 0.20$ m.

The rough bed was formed by placing a thick layer of sediments throughout the channel bed (Fig. 2). The sediment disposal in the channel was made in order to create a layer with thickness around $3D_{50}$, where D_{50} is the grain size diameter for which 50% of the sediments have smaller diameters, having herein the same meaning as the roughness scale ε. Table 1 summarizes the parameters of the experiments, where $g'_0 = g\Delta\rho/\rho_0$ is the reduced gravity, being g the acceleration of gravity and $\Delta\rho$ the density difference between the saline mixture and the ambient fluid.

The density of the saline water is controlled by a pycnometer being the error of the weighing apparatus 0.05%. A controlled quantity of white colorant is added to the mixture in the lock to provide flow visualization. The outside back wall of the channel is lined with black paperboard to produce a dark, uniform background to contrast with the white dyed developing gravity current.

Figure 2. Details of the rough beds used for runs of type R: R1 (left), R2 (center) and R3 (right). View of the channel bed from the downstream section, i.e., right end wall in Fig. 1.

Table 1. Main parameters of the experiments.

Run	ρ_1 ($\mathrm{kgm^{-3}}$)	ε (mm)	g'_0 ($\mathrm{ms^{-2}}$)	Symbols in figures
D2	1030	0.0	0.294	□
R1	1030	2.9	0.294	+
R2	1030	4.6	0.294	Δ
R3	1030	24.6	0.294	○

At the beginning of each experiment the gate is suddenly removed, leaving the dense fluid to flow under the fresh water. The evolution of the gravity current is recorded by a CCD video camera with 768×576 pixels of resolution and acquisition frequency of 25 Hz.

The camera is kept at a fixed perpendicular position 5.8 m from the channel and aligned with its centre to capture the entire channel length. A metric scale is positioned in both horizontal and vertical directions of the channel for geometric calibration purposes. The video frames were subsequently converted into gray scale matrices in the region of the channel with fluid and then converted into instantaneous width-averaged density fields of the current through a calibration procedure.

Eight known dye quantities, increasingly from zero to a maximum value corresponding to ρ_1, were uniformly distributed through the channel being the corresponding images captured for calibration for the very same light conditions and distance between camera and channel as during the experiments. Gray scale values increase nonlinearly with the amount of dye in the flow. Assuming a direct relation between the amount of dye and the density of the current (the dye introduces a negligible extra-density to the fluid of about 0.2%), it is thus possible to infer density values at any given pixel and at any given instant from its instantaneous gray scale value. The results from this procedure are then verified and eventually corrected through total salt mass conservation principle applied to the entire experimental channel, accounting thus with the current mass and the mass of ambient fluid.

Figure 3 shows the development of the current captured at $t = 22.5$ s ($t/t_0 = 36.4$, see further for the

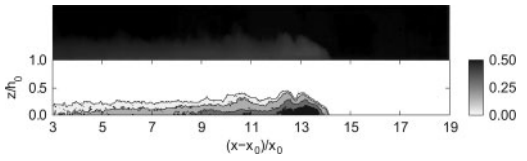

Figure 3. (top) Photo of the current acquired at $t = 22.5$ s ($t/t_0 = 36.4$) after the gate removal in run D2; (bottom) non-dimensional iso-density contours plotted at $\rho^* = 0.02$, 0.15, 0.30 and 0.50.

definition of t_0) after the gate removal for experimental run D2 and the correspondent plot of iso-density contours plotted for $\rho^* = 0.02$, 0.15, 0.30 and 0.50, being $\rho^*(x, z, t)$ the instantaneous 2D local non-dimensional density defined as

$$\rho^*(x,z,t) = \frac{\rho(x,z,t) - \rho_0}{\rho_1 - \rho_0} \tag{1}$$

where $\rho(x, z, t)$ is the local width-averaged density of the current. Flow depth is normalized by the initial depth at the lock, h_0, and streamwise distance is represented in terms of lock-lengths, $x - x_0/x_0$. The time after the gate removal is non-dimensionalized by

$$t_0 = \frac{x_0}{\sqrt{g_0' h_0}} \tag{2}$$

3 RESULTS

3.1 *Front velocity*

The current front velocity, u_f, was obtained by derivation in time of the regression functions adjusted to the time-varying front position (cf. Nogueira et al. 2011). In this procedure, the boundary of the current was defined as the non-dimensional iso-density contour of 0.02 (following Hacker et al. 1996). Two distinct phases were observed for the development of the current: a first phase characterized by the current front advancing at approximately constant velocity and a second phase where velocity decreases in time.

The dimensionless front velocity, i.e, Froude number, is herein defined as:

$$Fr_h = \frac{u_f}{\sqrt{g'_h h_m}} \tag{3}$$

being $g'_h = g(\rho_h - \rho_0)/\rho_0$ the local reduced gravity, where ρ_h is the head-averaged density of the current at each instant and h_m the maximum head height (cf. Fig. 5).

Figure 4 shows Froude numbers plotted for all runs. In general, Fr_h exhibits some scatter which is reduced in the second phase, i.e., after $(x_f - x_0)/x_0 = 9$ (self-similar phase observed in lock-exchange experiments, cf. Rottman & Simpson 1983). In particular, runs D2, R1 and R2 show a consistent collapse around

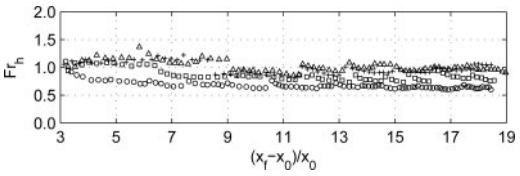

Figure 4. Evolution of Froude numbers for all runs (symbols explained in Table 1).

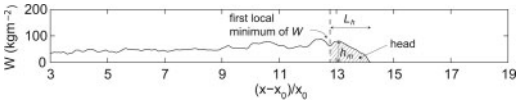

Figure 5. Definition of the head of the gravity current.

$Fr_h = 0.8$. This result is in agreement to what is reported in Marino et al. (2005). Run R3 shows an evident deviation from the remaining runs, exhibiting a tendency towards a lower value, $Fr_h = 0.6$. The difference observed in run R3 suggests that the additional bed drag induced by the higher bed roughness has a predominant effect in the current deceleration, with no apparent effect on density reduction.

The fact of having Froude number based on local parameters approximately constant leads to the conclusion that the current head is in local balance.

3.2 *Head definition*

To assess the local parameters at the current head, a criterion to isolate this region has to be established. This is not straightforward since the boundary and the inner structure of the current are highly unsteady. Previous contributions have shown that the head is the region where higher density is observed within the current (Marino et al. 2005, Hacker et al. 1996, Hallworth et al. 1996).

The criterion herein used to characterize and isolate the head region is based on a dynamic function given by the product between local values of depth-averaged density and current height:

$$W(x,t) = \overline{\rho_v}(x,t) \cdot h(x,t) \tag{4}$$

which corresponds to local vertically-averaged mass of the current (kgm^{-2}).

The upstream limit of the head, and therefore the head length L_h, was defined taking the position of the meaningful local minimum of function W nearer the current front. Accordingly, Figure 5 illustrates the definition of the head of the gravity current.

The head of the current constitutes the control volume herein analyzed. The estimation of head mass can thus be made through integration of the concentration values measured within this region.

3.3 *Head dynamics*

Figures 6 and 7 show the main results regarding head dynamics, namely the temporal evolution of the length,

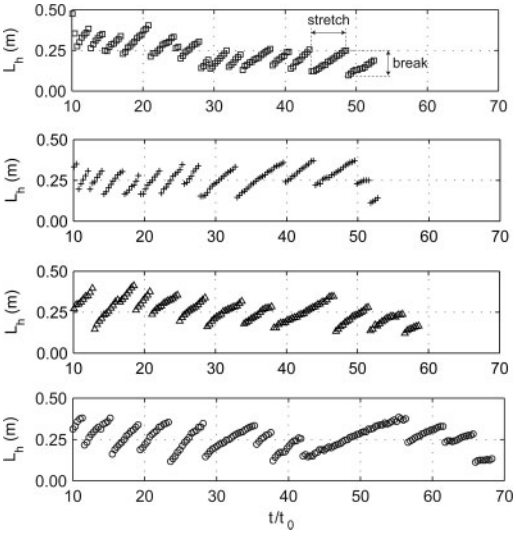

Figure 6. Length of the gravity current head for all runs (symbols explained in Table 1).

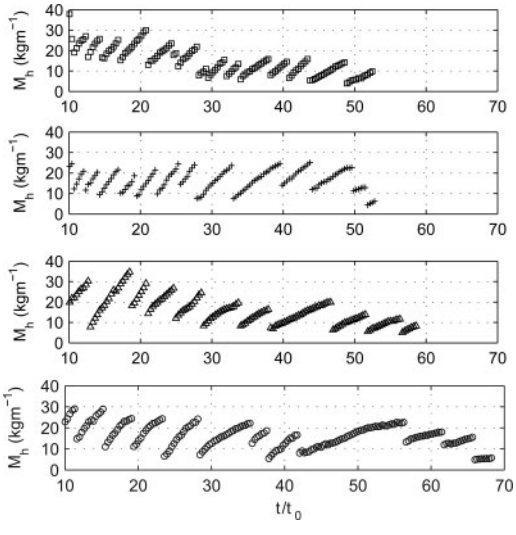

Figure 7. Mass of the gravity current head for all runs (symbols explained in Table 1).

L_h, and mass M_h per unit width of the gravity current head, plotted as function of dimensionless time, t/t_0, after the gate removal.

The temporal evolution of both length and mass show remarkable patterns characterized by successive events of stretching and breaking of the head (cf. top of Fig. 6). During the stretching phase, an increase both in length and mass of the head is observed due to entrainment of ambient fluid into the head region. The breaking cycles show that a limit exists in the entrainment capacity of the head, indicating an instability process eventually controlled by a dynamical quantity. After this limit is attained, the head breaks leaving behind *quasi*-steady large-scale billows, visible in Figure 3 at position $(x - x_0)/x_0 = 12.5$ for instance, which eventually fade in time by diffusion-type processes.

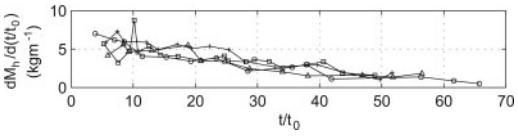

Figure 8. Mass rate within each stretching phase for all runs (symbols explained in Table 1).

Analyzing the period between two consecutive break events, given by $T^* = \Delta t/t_0$, we observe that the period is quite irregular within a run, i.e, no consistent evolution trend is observed. The average non-dimensional period for each run is $T^* = 2.4$ (D2), 3.0 (R1), 3.9 (R2) and 4.7 (R3), suggesting that as the bed roughness increases, the breaking events tend to occur less frequently and a temporal extension of the stretching phases occurs. A similar trend was observed when looking to the duration of the longest stretching event, i.e, the maximum period between breaks within each run: $T^* = 5.2$ (D2), 6.8 (R1), 8.8 (R2) and 14.4 (R3).

The temporal evolution of length (Fig. 6) and mass (Fig. 7) at the stretching phase of the head show an approximately linear trend. Figure 8 shows the temporal grow rate of mass, $dM_h/d(t/t_0)$, within each stretching phase, plotted as function of the non-dimensional time. In general, the growing rate decreases as the current advances, suggesting that the entrainment rate at the head is ruled by local reduced gravity: as current develops and ambient fluid is being entrained into the current head, local density decreases and so does local reduced gravity. This should tend to an equilibrium state, not seen in these experiments due to geometric constraints. Growing rates present a similar decaying evolution between the several tests.

Figure 9 shows the temporal evolution of the current mass normalized by the initial mass in the lock, M_0, and plotted as a function of dimensionless front position $(x_f - x_0)/x_0$. Figure 10 shows the spatial grow rate of mass, $dM_h/d((x_f - x_0)/x_0)$, within each stretching phase. In this plot, the growing rates are approximately constant in all runs during the first phase of the current development, i.e, for $(x_f - x_0)/x_0 < 9$. During the second phase a consistent overall decrease trend is observed in all runs. The average non-dimensional length scale for each run is $X^* = \Delta x/x_0$ and equal to 0.9 (D2), 1.0 (R1), 1.3 (R2) and 1.2 (R3).

4 CONCLUSIONS

An image analysis technique was used to investigate the dynamics of the head of lock-released gravity currents developing over smooth and rough beds.

Froude number obtained through local parameters show that the front velocity converges to a balance with the local buoyancy at the head.

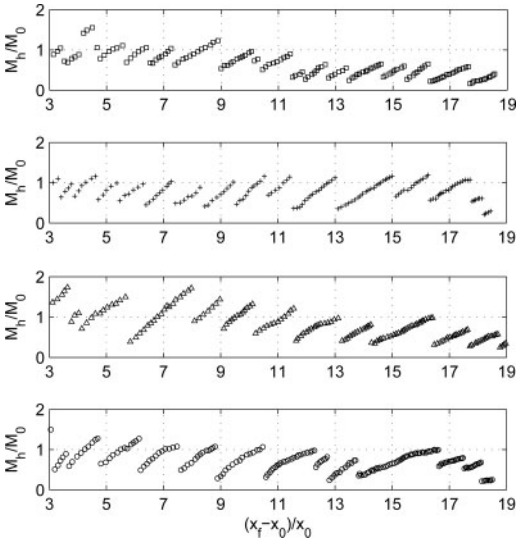

Figure 9. Mass per unit width of the gravity current head for all runs (symbols explained in Table 1).

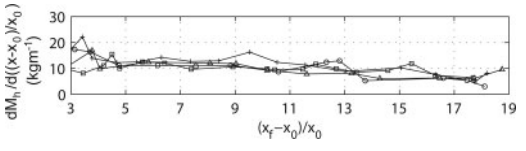

Figure 10. Mass spatial growth rate within each stretching phase for all runs (symbols explained in Table 1).

The temporal evolution of both length and mass at the head show repeated cycles of head stretching and breaking. During the stretching phase, ambient fluid is entrained into the head until that region becomes unstable and consequently breaks. These events are followed by *quasi*-steady large-scale billows that remain at the rear of the head, which eventually fade in time by diffusion-type processes. Bed roughness is seen to play an important role in this process: as roughness increases, besides the expected current deceleration, the breaking events become less frequent.

The rate of growth of length and mass within the stretching, or growth, phases is seen to decrease in time, which suggests that the entrainment phenomenon is ruled by local buoyancy. In particular, when plotted as a function of the dimensionless front position, the growing rate of mass is approximately constant during the first phase of the current development, decreasing substantially in the second, self-similar, phase.

ACKNOWLEDGMENTS

This research was supported by the Portuguese Science and Technology Foundation through the research project PTDC/ECM/099752/2008 and the research grant SFRH/BD/48705/2008.

REFERENCES

Adduce, C., Lombardi, V., Sciortino, G. & Morganti, M. 2009. Roughness effects on gravity currents dynamics. *Proc. 33rd IAHR Congress, Vancouver, 9–14 August 2009*.

Adduce C., Sciortino G. & Proietti S., 2012. Gravity currents produced by lock-exchanges: experiments and simulations with a two layer shallow-water model with entrainment, *J Hydr Eng* (in press).

Altinakar, M.S. 1993. Weakly depositing turbidity currents on small slopes, Ph.D. Thesis, École Polytechnique Fédérale de Lausanne (EPFL), Lausanne, Switzerland.

Alves, E., González, J., Freire, P. & Cardoso, A.H. 2008. Experimental study of plunging turbidity currents in reservoirs. *River Flow 2008, Çesme-Izmir, September, 2008.*

Bombardelli, F.A., Cantero, M.I., García, M.H. & Buscaglia, G.C. 2009. Numerical aspects of the simulation of discontinuous saline underflows: the lock-exchange problem. *J Hydr Res*, 47(6):777–789.

Fan, J. & Morris, G.L. 1992a. Reservoir sedimentation I: Delta and density current deposits. *J Hydr Eng*, 118(3):354–369.

Fan, J. & Morris, G.L. 1992b. Reservoir sedimentation II: Reservoir desiltation and long-term storage capacity. *J Hydr Eng*, 118(3):370–384.

Hacker, J., Linden, P.F. & Dalziel, S.B. 1996, Mixing in lock-release gravity currents, *Dyn Atmos Oceans*, 24:183–195.

Hallworth, M.A., Huppert, H.E., Phillips, J.C. & Sparks, R.S. 1996, Entrainment into two-dimensional and axisymmetric turbulent gravity currents. *J Fluid Mech*, 308:289–311.

Härtel, C., Meiburg, E. & Necker, F, 2000. Analysis and direct numerical simulation of the flow at a gravity-current head. Part 1. Flow topology and front speed for slip and no-slip boundaries. *J Fluid Mech,* 418:189–212.

Kantoush, S.A., Sumi, T. & Murasaki, M. 2010. Evaluation of sediment bypass efficiency by flow field and sediment concentration monitoring techniques. *Annual J Hydr Eng*, 55.

La Rocca, M., Adduce, C., Sciortino, G. & Pinzon, A.B. 2008. Experimental and numerical simulation of three-dimensional gravity currents on smooth and rough bottom. *Physics of Fluids*, 20.

Marino, B.M., Thomas, L.P. & Linden, P.F. 2005. The front condition for gravity currents. *J Fluid Mech*, 536:49–78.

Nogueira, H.I.S., Adduce, C., Alves, E. & Franca, M.J. 2011. Phase analysis of lock-exchange gravity currents. *Proc. 7th Int. Symp. on Stratified Flows, Rome, 22–26 August 2011.*

Oehy, C. & Schleiss, A. 2007. Control of turbidity currents in reservoirs by solid and permeable obstacles, *J Hydr Eng,* 133(6):637–648.

Ooi, S.K., Constantinescu, G. & Weber, L.J. 2007. 2D Large-eddy simulation of lock-exchange gravity current flows at high Grashof numbers. *J Hydr Eng*, 133(9):1037–1047.

Özgökmen, T.M. & Fischer, P.F. 2008. On the role of bottom roughness in overflows. *Ocean Modelling,* 20:336–361.

Paik, J., Eghbalzadeh, A. & Sotiropoulos, F. 2009. Tree-dimensional unsteady RANS modelling of discontinuous gravity currents in rectangular domains. *J Hydr Eng*, 135(6):505:521.

Parker, G., Fukushima, Y. & Pantin, H.M. 1986. Self-accelerating turbidity currents. *J Fluid Mech,* 171:145–181.

Peters, W.D. & Venart, J.E.S. 2000. Visualization of rough-surface gravity current flows using laser-induced fluorescence. *Proceedings of 9th International Symposium of Flow Visualization.* Edinburgh, 2000.

Rossato, R. & Alves, E. 2011. Experimental study of turbidity currents flow around obstacles. *Proceedings of 7th International Symposium on Stratified Flows. Rome, 2011.*

Rottman, J.W. & Simpson, J.E. 1983. Gravity currents produced by instantaneous releases of a heavy fluid in a rectangular channel. *J Fluid Mech*, 135:95–110.

Shin, J.O., Dalziel, B.S. & Linden, P.F. 2004. Gravity currents produced by lock exchange. *J Fluid Mech,* 521: 1–34.

Simpson, J.E. 1997. Gravity currents: in the environment and the laboratory. 2nd edn., Cambridge University Press, New York, pp 1–2.